Glass transitions in 1, 2, 3, and 4 dimensional binary Lennard-Jones systems

Ralf Brüning,[1,*] Denis A. St-Onge,[1] Steve Patterson,[1,2] and Walter Kob[3]

[1]*Physics Department, Mount Allison University, Sackville, New Brunswick, Canada E4L 1E6*

[2]*present address: Department of Physics and Atmospheric Science, Dalhousie University, Halifax, NS, Canada B3H 3J5*

[3]*Laboratoire des Colloïdes, Verres et Nanomatériaux, UMR5587, Université Montpellier II and CNRS, 34095 Montpellier Cedex, France*

(Dated: November 18, 2008)

Abstract

We investigate the calorimetric liquid-glass transition by performing simulations of a binary Lennard-Jones mixture in one through four dimensions. Starting at a high temperature, the systems are cooled to $T = 0$ and heated back to the ergodic liquid state at constant rates. Glass transitions are observed in two, three and four dimensions as a hysteresis between the cooling and heating curves. This hysteresis appears in the energy and pressure diagrams, and the scanning-rate dependence of the area and height of the hysteresis can be described by power laws. The one dimensional system does not experience a glass transition but its specific heat curve resembles the shape of the $D \geq 2$ results in the supercooled liquid regime above the glass transition. As D increases, the radial distribution functions reflect reduced geometric constraints. Nearest-neighbor distances become smaller with increasing D due to interactions between nearest and next-nearest neighbors. Simulation data for the glasses are compared with crystal and melting data obtained with a Lennard-Jones system with only one type of particle and we find that with increasing D crystallization becomes increasingly more difficult.

PACS numbers: 64.70.Pf, 42.70.Ce, 61.10.Eq

*rbruening@mta.ca, Tel.: (506) 364-2587, Fax.: (506) 364-2583

I. INTRODUCTION

As a glass-forming liquid is cooled, its relaxation time increases very rapidly and at sufficiently low temperatures, the relaxation time eventually exceeds the time scale of cooling. Thus, provided that crystallization is avoided, the system forms a glass at a temperature T_g and due to the kinetic effects the non-equilibrium state of this glass depends on its thermal history [1, 2, 3, 4, 5, 6, 7, 8, 9, 10, 11, 12, 13, 14, 15]. In recent years much theoretical effort has been made to gain a better understanding of the mechanism(s) responsible for the dramatic slowing down of the relaxation dynamics as well as to investigate the aging dynamics of the system once the system has fallen out of equilibrium [16, 17, 18, 19, 20, 21, 22, 23]. Most of these studies have been done for three dimensional systems since this correspond to the overwhelming majority of real experiments, with some notable exceptions in which the (experimental) glass transition has been investigated in quasi-two dimensional systems [24, 25]. Fewer investigations have been devoted to the question to what extend the phenomenon of the glass transition depends on the dimensionality of the system since experimentally it is rather difficult to change the dimensions without modifying the interactions. Nevertheless, such a study is of interest, since it allows one to estimate the role of the local geometry on the glass-forming ability of the system. Although it is evident that with increasing dimensionality D the geometric constraints decrease, it is difficult to estimate this tendency within an analytical calculation in a more quantitative way [26, 27, 28]. One possibility to address the problem is to use computer simulations to determine, with a given interaction potential, the dependence of the thermodynamic and structural properties of the system as a function of D.

In the present paper we study therefore how the glass transition of a binary-mixture Lennard-Jones (BMLJ) system depends on its dimensionality D. In the past it has been shown that such a system shows, for $D = 3$, many properties of real glass formers and thus it can serve as a good model for glass-forming systems [10, 29, 30, 31, 32, 33, 34, 35, 36, 37, 38]. Here we will focus on the details of the glass transition as characterized by the specific heat measurements, we will examine the structure of this system in its glassy state and we will compare the results with experimental data. Note that here we will not discuss the relaxation dynamics and we refer to Refs. [39, 40, 41, 42, 44, 45] in which such investigations have been done for two-dimensional systems.

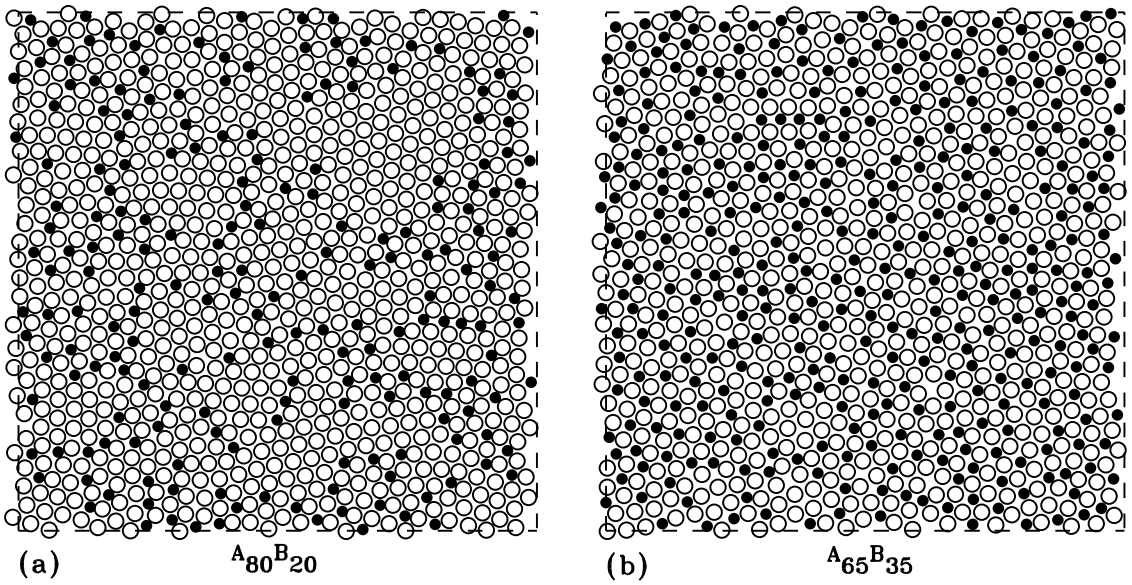

FIG. 1: Typical configurations of the $A_{80}B_{20}$ (a) and $A_{65}B_{35}$ (b) systems for $D = 2$ at $T = 0$. These systems have been cooled to $T = 0$ with cooling rates $\gamma = -1.0 \times 10^{-5}$ and $\gamma = -1.0 \times 10^{-7}$, (a) and (b) respectively. Open and filled disks represent A and B particles, respectively. Dashed lines indicate the (virtual) boundary of the simulation box.

Section II of this paper discusses the details of the simulation, including the type of system and the method by which it is studied. Section III describes the results of the simulations, starting with microscopic properties of the system, moving to the macroscopic properties. Concluding remarks are given in Section IV.

II. MODEL AND DETAILS OF THE SIMULATIONS

Following previous work, we consider a binary mixture of particles A and B, all having the same mass, m [29, 30, 31]. We extend the usual three-dimensional BMLJ molecular dynamics simulation to one ($D = 1$) through four ($D = 4$) spatial dimensions. A number of particles, N, is placed inside a box with edge length L and constant volume $V = L^D$. As in previous work, periodic boundary conditions are imposed [46]. The interactions between particles are given by the Lennard-Jones potential, $U_{\alpha\beta}(r) = 4\epsilon_{\alpha\beta}[(\sigma_{\alpha\beta}/r)^{12} - (\sigma_{\alpha\beta}/r)^6]$, where $\alpha, \beta \in \{\mathrm{A}, \mathrm{B}\}$, $\sigma_{\mathrm{AA}} = 1.0$, $\epsilon_{\mathrm{AA}} = 1.0$, $\sigma_{\mathrm{AB}} = 0.8$, $\epsilon_{\mathrm{AB}} = 1.5$, $\sigma_{\mathrm{BB}} = 0.88$ and $\epsilon_{\mathrm{BB}} = 0.5$ [29]. Here r is defined through $r^2 = \sum_{k=1}^{D} x_k^2$, where x_k is the k^{th} cartesian component of the inter-particle separation. Following common practice, the potential is truncated and

shifted at $r = 2.5\sigma_{\alpha\beta}$ [29, 46]. Reduced units are used, with $\sigma_{\rm AA}$ being the unit of length, $\epsilon_{\rm AA}$ the unit of energy, $(m\sigma_{\rm AA}^2/48\epsilon_{\rm AA})^{1/2}$ the unit of time [29], and Boltzmann's constant, k_B, is set equal to one. The temperature, T, is controlled by a Nosé-Hoover thermostat [46] with an effective mass of 48 reduced units. For the molecular dynamics of the particles, the equations of motion are integrated using the Verlet algorithm with a time step of 0.02 [29]. The pressure, P, is monitored using the virial theorem, $PV = NT + D^{-1}\sum_{i<j}\mathbf{f}_{ij}\cdot\mathbf{r}_{ij}$, where $\mathbf{f}_{ij}$ is the force and $\mathbf{r}_{ij}$ the separation between particles i and j.

Part of the simulations were carried out for the composition $A_{80}B_{20}$ in three dimensions, a system that has been studied extensively [29, 30, 31, 32, 33, 34, 35, 36, 37, 38]. For $D = 1, 2, 3$, and 4, the composition $A_{65}B_{35}$ was selected because it is, unlike $A_{80}B_{20}$, stable against crystallization for $D = 2$ at the cooling rates employed here. All simulations begin with the system in equilibrium at a sufficiently high initial temperature. The temperature is lowered at the rate $-\gamma$ to $T = 0$ and then increased back to the initial temperature at the rate γ, where $\gamma = 1.0 \times 10^{-3}$, 1.0×10^{-4}, and 1.0×10^{-5}. Further simulations with $\gamma = 1.0 \times 10^{-6}$ have been performed for $D = 2, 3$, and for $D = 2$ additional simulations were carried out at $\gamma = 1.0 \times 10^{-7}$. The $A_{80}B_{20}$ system was studied with γ in the range from $\gamma = 1.0 \times 10^{-3}$ to $\gamma = 1.0 \times 10^{-7}$. For $D = 1, 2$, and 3 the number of particles is $N = 1000$, while N is 2000 for $D = 4$. To increase the statistical significance of the results, data are averaged over independent runs with different initial configurations. At the starting temperatures the relaxation times are very short, equilibrium is rapidly attained and the statistically independent starting configurations are readily obtained. The starting configurations for $D = 1$ simulations are random sequences of A and B particles. In general the results represent averages over 100 runs. Due to computation time constraints, only 20 runs are used for the $D = 4$, $A_{65}B_{35}$ system as well as for $A_{80}B_{20}$ with $\gamma \leq 1.0 \times 10^{-6}$.

The particle density ρ for the $A_{80}B_{20}$ simulations is the same as in previous work with $L = 9.4$ in $D = 3$, i.e. $\rho = N/L^D = 1.204$ [29]. To establish a common reference point for all $A_{65}B_{35}$ systems at different dimensionalities, the system volume was chosen such that the simulation pressure is approximately zero when the temperature reaches $T = 0$ upon cooling at $\gamma = -1.0 \times 10^{-4}$. The resulting box edge lengths are $L = 1002.5$, 29.34, 8.88 ($N = 1000$) and 5.68 ($N = 2000$) for $D = 1, 2, 3$ and 4, respectively. It has been shown that the bulk properties of $D = 3$ BMLJ systems emerge with as few as 65 particles [43].

Further simulations with only A particles (A_{100}) were carried out in order to identify the

features that distinguish the vitreous from the crystalline state. Box sizes, adjusted such that $P \approx 0$ for the crystalline state at $T = 0$, are 1119 ($N = 1000$), 32.7 ($N = 1000$), 9.85 ($N = 1000$), and 6.0639 ($N = 2048$) for $D = 1$ to 4. Temperature scanning rates ranged between $\gamma = \pm 1.0 \times 10^{-3}$ and $\pm 1.0 \times 10^{-4}$. The $D = 2$ and $D = 3$ systems crystallize spontaneously upon cooling whereas the $D = 4$ remained in a metastable state. Therefore the $D = 4$ system was heated from an initially prepared fcc crystal consisting of 4^4 unit cells that each contain 8 particles with 24 equidistant neighbors [47].

III. RESULTS AND DISCUSSION

Since we are interested in the phenomenon of the glass transition, we have to consider the stability of the model system against crystallization. Figure 1a shows a typical configuration of the particles for the $A_{80}B_{20}$ composition, in two dimensions, cooled to $T = 0$ at a rate of -1.0×10^{-5}. As observed previously for a similar system [48], the configuration contains areas of hexagonally crystallized A particles in a matrix of amorphous AB material, i.e. the system which is a good glass-former in three dimensions is crystallizing in two dimensions. In order to suppress these hexagonal A crystals for $D = 2$, we selected the composition $A_{65}B_{35}$. Figure 1b shows a typical configuration of a $A_{65}B_{35}$ system which has been cooled to $T = 0$ at a rate of -1.0×10^{-7}, the slowest rate employed in this study. The structure appears to be fully amorphous, as required. In the following we will first discuss the results obtained for the $A_{65}B_{35}$ composition. Commonalities and differences between $A_{65}B_{35}$ and $A_{80}B_{20}$ for $D = 3$ will be considered at the end of this section.

In Fig. 2(a) we show the temperature dependence of the pressure for different values of D. The $P(T)$ curves are approximately linear, and their slope increases with the dimensionality. Recall that the particle density is adjusted for each dimension such that $P \approx 0$ as the temperature reaches $T = 0$ upon cooling at $\gamma = -1.0 \times 10^{-4}$ (see Sec. II). Actual pressures obtained after cooling to $T = 0$ at this rate are between -0.10 and 0.00. Cooling the system more slowly results in a more relaxed glass state, i.e. a more efficient packing of the particles and thus a lower pressure at $T = 0$. For the rate $\gamma = -1.0 \times 10^{-5}$ (Fig. 2), pressures range from -0.59 ($D = 4$) to 0.00 ($D = 1$). Pressures at $T = 0$ are small compared with pressures at T_g, with $|P(T = 0)|$ less that 5% of $P(T_g)$, as required for consistency.

The figure also shows that there is a hysteresis between the cooling curve and the heating

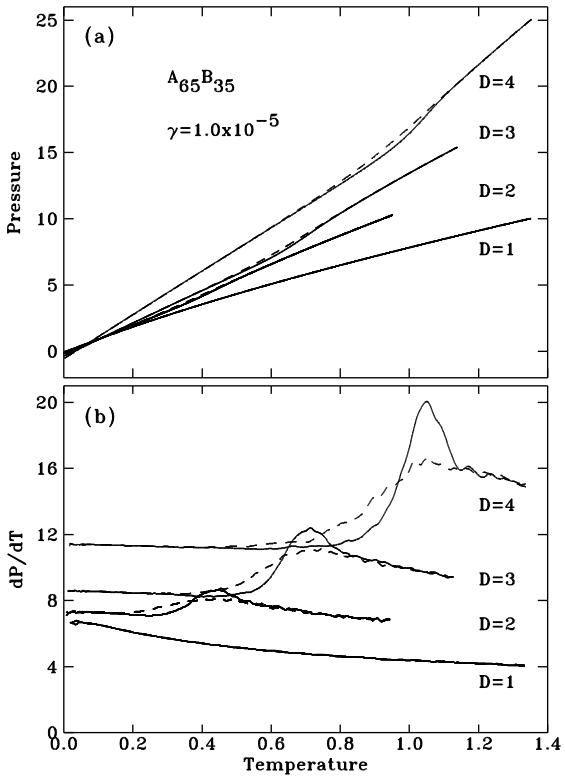

FIG. 2: (a) Temperature dependence of the pressure of the $A_{65}B_{35}$ systems for $D = 1$ to $D = 4$ upon cooling (dashed lines) followed by heating (solid lines) at $\gamma = \mp 1.0 \times 10^{-5}$. (b) Temperature derivatives of the same pressure data.

curve for $D \geq 2$, which becomes more pronounced as D increases. This hysteresis is seen more clearly in the temperature derivative of the pressure, dP/dT (Fig. 2(b)). As it will be discussed below, the glass transition temperatures for the data shown in Fig. 2 are $T_g = 0.33,\ 0.58$, and 0.89 for $D = 2, 3, 4$, respectively. These values for T_g were obtained by first calculating the fictive temperature of the system, $T_f(T)$, as defined by Tool [49]. The procedure is based on analytic approximations for the specific heat of the supercooled liquid [50] and the glass (further details are given below). In the liquid state the fictive temperature equals the temperature, while in the glass state it becomes frozen at a finite value. We set $T_g = T_f(0)$, the limiting value of the fictive temperature as the glass stops evolving upon cooling to low temperatures.

Above the temperature range of this hysteresis loop, the system is in equilibrium and the pressures upon cooling and heating coincide. A hysteresis is a hallmark of physical glasses in the glass transition range [51] and the glass transition found here is qualitatively

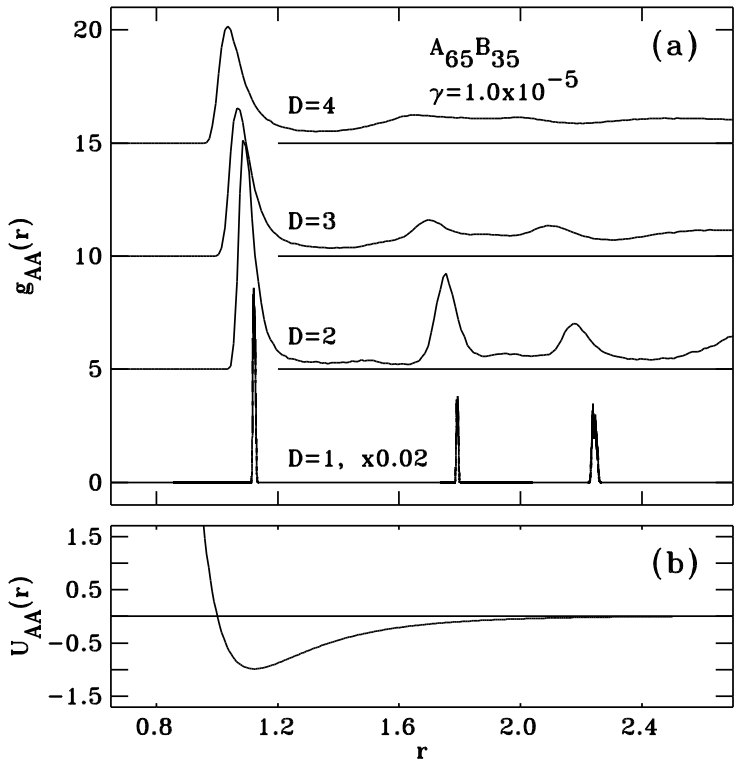

FIG. 3: (a) Radial distribution of A–A pairs for $A_{65}B_{35}$ cooled to $T = 0$ at the rate -1.0×10^{-5}. Data for $D = 1$ are multiplied by 0.02. Data for $D \geq 2$ are shifted up successively by 5. (b) Lennard-Jones potential for A–A interaction, truncated and shifted at $r = 2.5$.

consistent with previous observations of a glass transition in cooling curves obtained with a $D = 3$, $A_{80}B_{20}$ BMLJ system [10]. Last not least we remark that the $D = 1$ system does not show any sign of a glass transition since in one dimension this Lennard-Jones model is not sufficiently frustrated to form a glass. (However, other one-dimensional models can show a glass transition, see, e.g., Ref. [52].)

In order to characterize the local structure of the particles it is useful to consider the radial pair distribution functions, $g_{\alpha\beta}(r)$, defined by [53]

$$g_{\alpha\beta}(r) = \frac{L^D}{F(r,D)N_\alpha N_\beta} \sum_{i\in\{\alpha\}} \sum_{j\in\{\beta\}} \langle \delta(r - r_{ij}) \rangle \quad , \tag{1}$$

where N_α is the number of particles of type α, r_{ij} is the distance between particle i and j, and the factor $F(r, D)$ normalizes $g_{\alpha\beta}(r)$ to 1.0 for large r, i.e. $F(r, 1) = 2$, $F(r, 2) = 2\pi r$, $F(r, 3) = 4\pi r^2$, and $F(r, 4) = 2\pi^2 r^3$.

Figures 3a, 4a, and 5a show the A–A, A–B and B–B distributions, respectively, at $T = 0$.

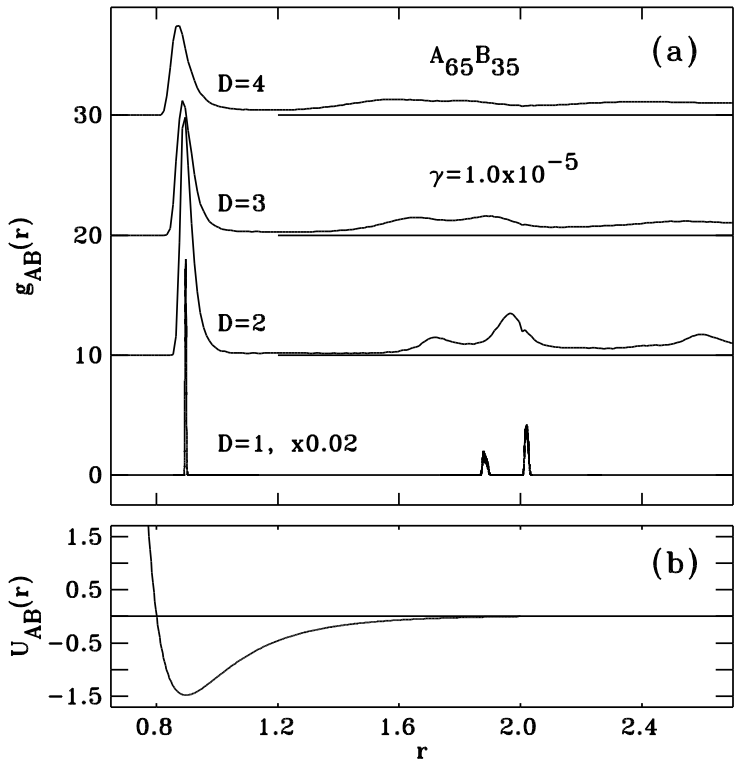

FIG. 4: (a) Radial distribution of A–B pairs for $A_{65}B_{35}$ cooled to $T = 0$ at the rate -1.0×10^{-5}. Data for $D = 1$ are multiplied by 0.02. Data for $D \geq 2$ are successively shifted up by 10. (b) Lennard-Jones potential for A–B interactions, truncated and shifted at $r = 2.0$.

For $D = 1$ one finds a first peak in $g_{\alpha\beta}$ at a distance $\sigma_{\alpha\beta}2^{1/6}$, i.e. at the location of the minimum in the corresponding pair potential (shown in panel b of the figures). This is due to the fact that we have adjusted the pressure to be zero at $T = 0$. The second and third A–A peaks in Fig. 3a for $D = 1$ are at $r = 1.80$ and $r = 2.25$ and correspond to $\underline{\text{A}}\text{B}\underline{\text{A}}$ and $\underline{\text{A}}\text{A}\underline{\text{A}}$ elements of the particle chain, respectively, where the underlined letters indicate the atom types considered in the pair distribution. For $g_{\text{AB}}(r)$ for $D = 1$, chain elements of the types $\underline{\text{A}}\text{B}\underline{\text{B}}$ and $\underline{\text{A}}\text{A}\underline{\text{B}}$ give rise to the peaks at $r = 1.89$ and $r = 2.03$, respectively. The $D = 1$ B–B radial distribution peaks are due to, in order of increasing r, $\underline{\text{BB}}$, $\underline{\text{B}}\text{A}\underline{\text{B}}$ and $\underline{\text{B}}\text{B}\underline{\text{B}}$ chain elements.

For $D = 2$, the peak at $r = 1.76$ corresponds to A–A next-nearest neighbors that are separated by a nearest neighbor particle of type B, while the peak at $r = 2.20$ correspond to A particles which are separated by a nearest neighbor particle of type A. The $D = 2$ peaks at $r = 1.73$ and $r = 1.96$ in the A–B distribution, Fig. 4, can be interpreted in a similar fashion and correspond to correlations with two A and two B nearest neighbors, respectively.

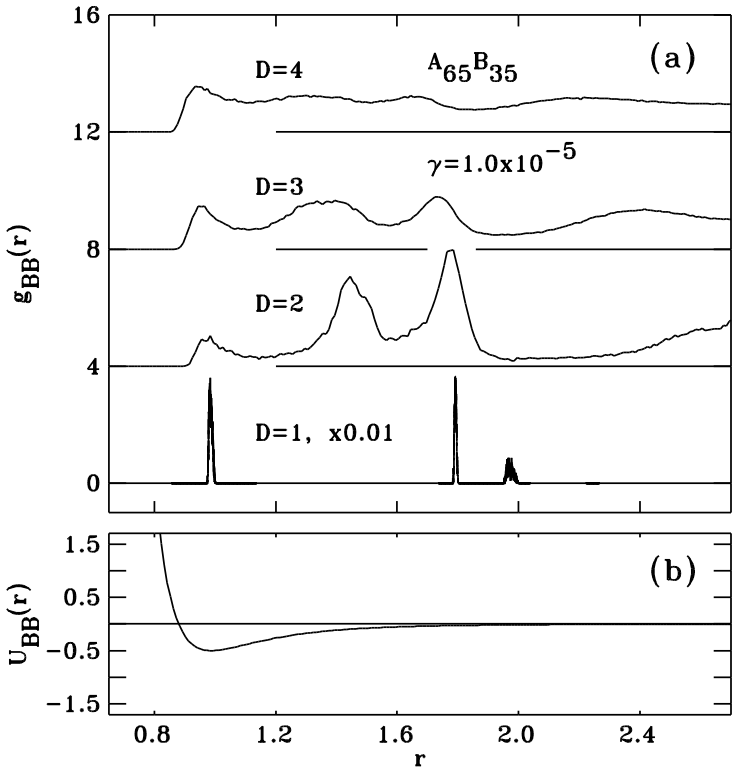

FIG. 5: (a) Radial distribution of B–B pairs for $A_{65}B_{35}$ cooled to $T = 0$ at the rate -1.0×10^{-5}. Data for $D = 1$ are multiplied by 0.01. Data for $D \geq 2$ are successively shifted up by 4. (b) Lennard-Jones potential for B–B interactions, truncated and shifted at $r = 2.2$.

In $g_{\rm BB}(r)$ a new B–B peak arises from the long edge of rectangles formed by four B particles surrounding an A particle, see Fig. 1(b).

We also mention that a notch can be seen in $g_{\rm AB}$ for $D = 2$ at $r = 2.0$, the point where the force is discontinuous due to the truncation of the potential [46]. It is unlikely that this discontinuity has a significant impact on the results.

The functions $g_{\alpha\beta}(r)$ also show a well defined nearest neighbor peak for $D = 3$ and 4, but the peaks at larger distances for these dimensions are much less pronounced than the ones found for $D = 1$ and 2, and it becomes difficult to associate them with particular arrangements of particles. Note that also the first nearest neighbor peak becomes broader with increasing D since the typical distance between neighboring particles will, at large D, be strongly influenced by the type and the number of the particles that are their common nearest neighbors. For the A–A correlation the increase of D will, e.g., make it possible that two A particles share an increasing number of B particles as first nearest neighbors

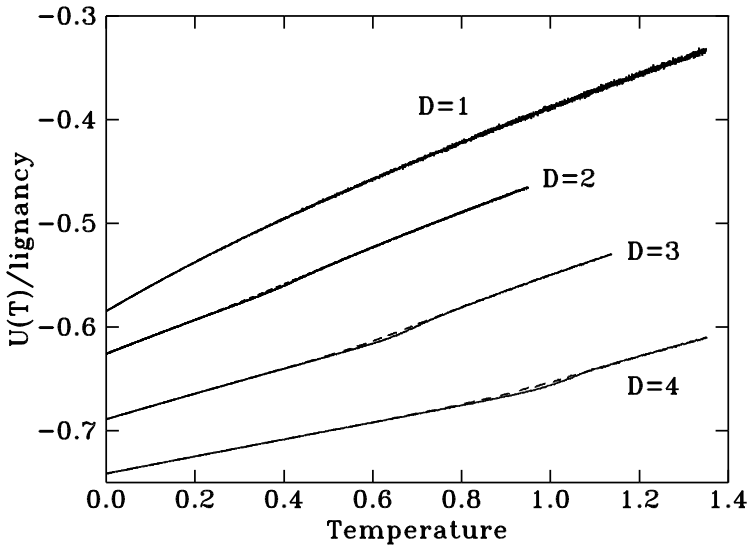

FIG. 6: Potential energy per particle versus temperature for $A_{65}B_{35}$ upon cooling (dashed lines) followed by heating (solid lines) at $\gamma = \mp 10^{-5}$. Potential energies are divided by the number of neighbors in a closely packed structure (lignancy = 2, 6, 12 and 24 for $D = 1$, 2, 3, 4, respectively).

and, since the A–B interaction is strongly attractive, thus decrease the nearest neighbor distance of such an A–A pair. Alternatively an A–A nearest neighbor pair that shares many A particles as first nearest neighbors, will have a distance that is somewhat larger than the average nearest neighbor A–A distance.

This mechanism for reducing the geometric constraints between particles that are nearest neighbors affects of course also the second, third,... -nearest neighbor configurations. This is the reason why with increasing D the radial distribution functions become less structured at a given r. In particular the location of the second, third,...-nearest neighbor peaks will shift to smaller distances and also the minima between consecutive peaks will be be less pronounced. This change in the geometry has the effect that the pressure of the system increases since the second nearest neighbor particles move to distances in which the potential is steeper/more attractive and hence the virial increases.

Having discussed the influence of the dimensionality on the structure we now present the results regarding the glass transition. One convenient method to investigate this transition in real glasses are specific heat measurements. We will consider the temperature dependence of the specific heat and energy of the BMLJ system. (See Refs. [10, 11, 12, 13, 14, 54, 55] for a discussion how other quantities depend on the cooling rate.) Figure 6 shows the potential

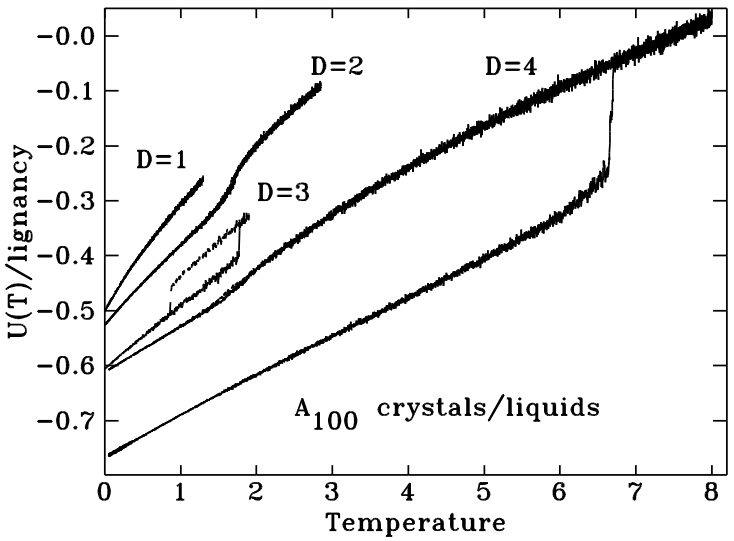

FIG. 7: Potential energy per particle versus temperature for systems containing only type A particles upon cooling (dashed lines) followed by heating (solid lines) at $\gamma = \mp 10^{-4}$ for $D = 1$, 2 and 3. Data for $D = 4$ were obtained at $\gamma = \pm 10^{-3}$ by heating and melting a closed-packed four-dimensional face-centered cubic crystal (lowest curve), followed by cooling and heating. Potential energies are divided by the number of neighbors in a closely packed structure (lignancy = 2, 6, 12 and 24 for $D = 1$, 2, 3, 4, respectively).

energy per particle for $A_{65}B_{35}$ as a function of temperature. For ease of comparison the potential energies are scaled by the number of nearest neighbors in closed-packed sphere structures. These lignancy values are 2, 6, 12 and 24 for $D = 1$ to $D = 4$ [47]. At $T = 0$, $P \approx 0$ the interaction energy of an isolated pair of A particles is 0.5. From Fig. 6 we recognize that for the $A_{65}B_{35}$ system the actual values are lower due to the higher A–B binding energy and the contributions of the next-nearest neighbor interactions. Total energies per particle (not shown) are negative, indicating bound states. The slopes of the $U(T)$/lignancy curves decrease with increasing D, reflecting enhanced cohesion and stability of the glass and liquid states per neighbor-pair.

First-order melting and crystallization are distinct from the glass transition. This is shown in Fig. 7 for constant-volume systems composed entirely of A particles. Box sizes were adjusted such that $P \approx 0$ for the crystalline state at $T = 0$, and in order to compare the curves for the different values of D we have divided them by the corresponding lignancy. (Note that since the binary system is a good glass-former, its crystalline structures are very

complex and not really known [56, 57].) For $D = 1$, the $T-$dependence of the potential energy of the chain similar to that of the random $A_{65}B_{35}$ chain, and no phase transition occurs for $T > 0$, as expected. In this case $U(T = 0)/2$ is 0.5, as expected, since next-nearest neighbor interactions are insignificant. The two-dimensional system crystallizes readily upon cooling near $T = 1.7$, and upon reheating melting nearly coincides with the crystallization. Upon cooling the $D = 3$ system stays in a (metastable) supercooled state down to a temperature $T \approx 0.9$ at which it crystallizes. The melting of the resulting crystal is observed at around $T = 1.8$, i.e. at about twice the temperature of crystallization. (Note that the exact values for melting and crystallization are probably affected by finite size effects. Furthermore one should recall that the resulting ordered structure does not have a long range positional ordering. However, these two issues are not that relevant here.)

Interestingly we found that for $D = 4$ the pure A system would not crystallize spontaneously. Therefore we assembled a dense-packed crystalline face-centered cubic structure with 4^4 unit cells of eight particles (2048 particles altogether, each with 24 equidistant nearest neighbors) [47]. Figure 7, lowest curve, shows that this structure melts at $T \approx 6.6$. Once melted, the $D = 4$ system does not crystallize upon cooling but instead forms a glass near $T = 1.5$ (heating and cooling data are shown). We conclude that with increasing D spontaneous crystallization becomes increasingly inhibited, i.e. the glass-forming ability increases with D. This trend is in agreement with the conclusions we drew in the discussion of the radial distribution functions (Figs. 3, 4, and 5), i.e. that the number of possible local packings increases rapidly with D and this entropic factor will make crystallization more difficult.

From Figure 7 we also recognize that at $T = 0$ the potential energy per lignancy decreases monotonically with D for liquids as well as for the glasses, in agreement with the trend observed for the binary mixture, Fig. 6. This results reflects the fact that the next-nearest neighbor atoms move closer to the central atom as D increases and hence lower their potential energy. The liquid state is characterized by a strong negative curvature of the $U(T)$ curves, while the curvature is much less for the crystal and glass states for $D = 2$, 3 and 4.

The specific heat at constant volume, $c_V = dE/dT$, is shown in Fig. 8a. The law of Dulong-Petit requires that for classical solids $\lim_{T\to 0} c_V(T) = D$ [58] and we find that the specific heat becomes indeed equal to D as temperature approaches zero. Also included in the graph is the $T-$dependence of the specific heat of the A_{100} crystals. At low T the specific heat of the

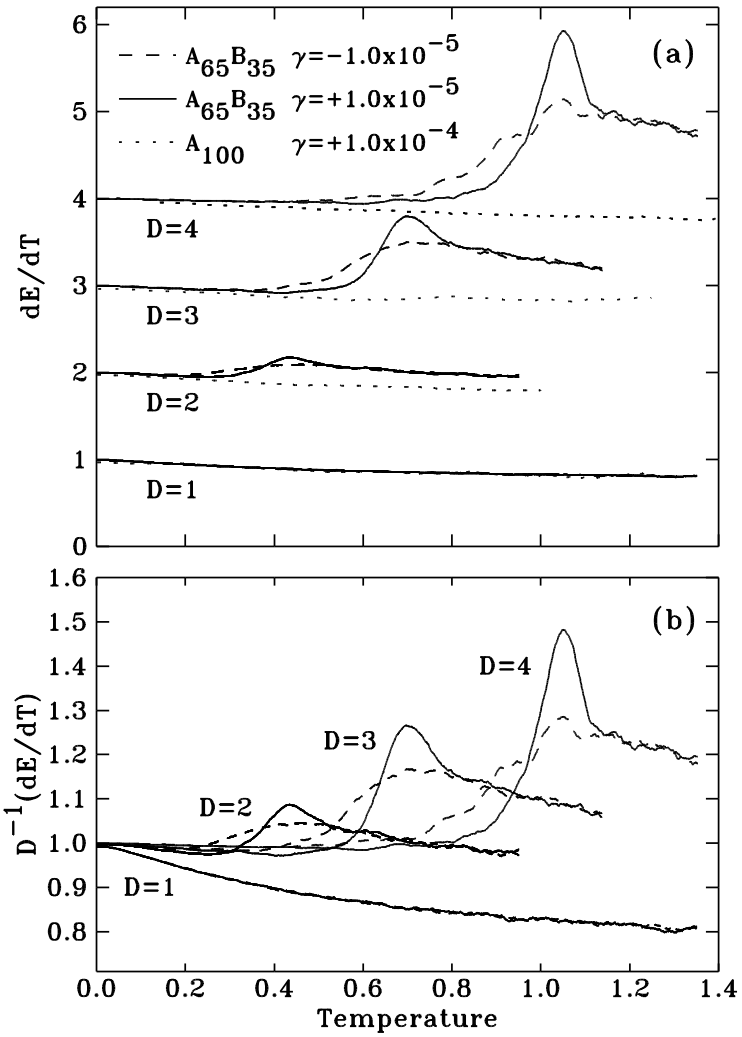

FIG. 8: (a) Constant volume specific heat, per particle, for $A_{65}B_{35}$ upon cooling (dashed lines) followed by heating (solid lines) at $\gamma = \mp 1.0 \times 10^{-5}$. The dotted lines show the specific heat of crystallized A particles upon heating at $\gamma = +1.0 \times 10^{-4}$. The cooling data for the crystals (not shown) coincide with the data upon heating. (b) Same data as in (a) but now divided by the dimension D.

glasses and and the crystals decreases with increasing temperature. This decrease is due to the anharmonicity of the effective potentials near the equilibrium positions of the particles. To see this we consider this effect in detail for the $D = 1$ case. For a chain segment with only one type of particle the first three terms of a Taylor expansion of the effective interparticle potential are given by $U(r) = U_0 + sr^2/2 + \lambda r^4$, where $U_0 < 0$ is the binding energy at $T = 0$. The quadratic term, with $s > 0$, leads to the nearly harmonic motion of the particle around its equilibrium position that gives rise to the Dulong-Petit result. The leading anharmonic

term has a positive coefficient ($\lambda > 0$) due to the repulsive interaction of the Lennard-Jones potential as neighboring particles approach. For a one-particle anharmonic oscillator of mass m the classical limit of the quantum-mechanical result [59] is

$$C = 1 - 6\lambda(m/s)^2 k_B T. \tag{2}$$

The negative term shows that the specific heat decreases in the vicinity of $T = 0$. However, the one-particle calculation on which Eq. (2) is based overestimates the decrease of the specific heat of the $D = 1$ particle chain by about a factor of two. This discrepancy is due to the multi-particle effects in a linear chain. Although it is unfortunately not possible to take into account these effects in an exact way, there exist approximation schemes to calculate them [60, 61] and it is found that at low T the specific heat does indeed decrease linearly with increasing T. These calculations also show that such a $T-$dependence is only found in the specific heat at constant volume, whereas the one at constant pressure increases with increasing T [61].

Figure 8a shows that for $D = 1$ the specific heat of the disordered glass coincides within the numerical accuracy of the data with the one from the crystal, i.e. the anharmonic effects in the two systems are very similar, at least in the $T-$range considered. The $c_V(T)$ data for the ($D = 1$) glass agrees with the one of the corresponding crystal not only in the $T-$range in which there is a linear $T-$dependence, but also at temperatures at which $c_V(T)$ is no longer linear. This is thus evidence that these two systems have also similar higher order anharmonic effects.

Similar results are obtained for the case of two dimensions for which we can compare the specific heat of the glass at low temperatures with that of a hexagonal crystals consisting solely of A particles, Fig. 8a. Type A particles by themselves crystallize readily, typically with about 2 vacancies per 1000 A particles, and the specific heat curves upon cooling and heating at $\gamma = \mp 10^{-4}$ agree with each other (data not shown). We see that up to $T = 0.2$ the specific heats of the hexagonal A phase and $A_{65}B_{35}$ glass nearly coincide. Therefore we can conclude that the linear decrease of the specific heat is not just a particularity of the glassy state, but instead a general property of both types of condensed Lennard-Jones systems at low temperatures. Qualitatively the same results are obtained for $D = 3$ and $D = 4$. This observation is in agreement with experimental findings since there it has been found that it is advantageous to crystallize samples *in situ* after measuring their specific

heats in the supercooled liquid and glassy states. By subtracting the measured specific heat of the crystal one obtains the net glass and supercooled liquid signals, and the net glass signal is typically indistinguishable from zero [62].

The excess specific heat is defined as $\Delta c_V(T) = c_V^{\rm liquid}(T) - c_V^{\rm glass}(T)$, where $c_V^{\rm liquid}$ is the specific heat of the system on the (metastable) liquid branch and $c_V^{\rm glass}$ is the specific heat of the frozen (non-ergodic) glass. At T_g we observe a step $\Delta c_V(T_g)$ as the system switches between the two states. This step and the hysteresis between heating and cooling characterizes the glass transition. As with the $P(T)$ curves, see Fig. 2, we find no step or hysteresis in Δc_V for $D = 1$. However, for $D \geq 2$ the glass transition can be readily be identified, and we see that T_g increases as the dimensionality increases. This rise of T_g with D is consistent with the higher binding energies per nearest neighbor particle pair (Fig. 6). Also the amplitude of the hysteresis increases with D, Fig. 8a. In Fig. 8b we normalize $c_V(T)$ by D, the specific heat at $T = 0$. Even with this normalization both $\Delta c_V(T_g)$ and the area of the hysteresis loop increase with D, reflecting the larger number of steric degrees of freedom when the particles can move in more dimensions.

Figure 8 also shows that above $T_g(D)$ the shape of the $c_V(T)$ curves are independent of D. This similarity of the specific heat suggests that, in terms of their thermal fluctuations, $D = 1$ particle chains behaves like a fluid down to $T = 0$. This observation is in agreement with analytical calculations for soft-sphere systems which find that 2.0 is the minimum (fractional) dimension required for a glass transition [26]. The absence of a transition for $D = 1$ may be linked to the fact that the $A_{65}B_{35}$ chains are non-erodic, since the initial random order of the particles in the chains remains fixed. Upon cooling these chains cannot reach an energetically favorable state with a higher number of nearest A–B neighbors, while the systems in higher dimensions can reach such chemically more ordered states.

Since the glass transition is related to the fact that the system falls out of equilibrium, the specific heat curves will, at temperatures around T_g, depend on the cooling and heating rate. In Fig. 9a we show the specific heat of the $A_{65}B_{35}$ mixture in three dimensions using temperature scanning rates that are varied by three orders of magnitude. As in real experiments [1, 2, 3, 5, 7, 63], T_g decreases with cooling rate. In Fig. 9b we show $c_V(T)$ for the $A_{80}B_{20}$ composition, using scanning rates that vary by four decades. Although at a first glance the data for the two compositions look quite similar, there are significant differences. Firstly in the $A_{65}B_{35}$ system the difference between the heating and cooling curves is larger

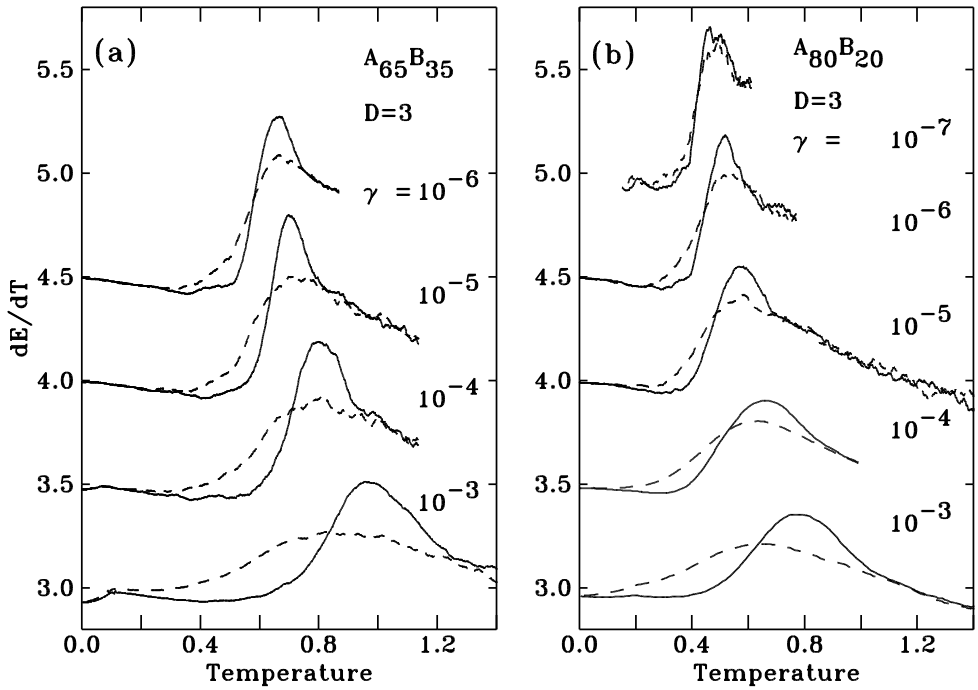

FIG. 9: Constant volume specific heat, per particle, of (a) $A_{65}B_{35}$ and (b) $A_{80}B_{20}$ for $D = 3$ upon cooling (dashed lines) followed by heating (solid lines). Curves at rates less than $\gamma = 10^{-3}$ are shown successively shifted up by 0.5.

than in the case of $A_{80}B_{20}$. This difference may be related, see the discussion of Fig. 1, to a higher concentration of locally frustrated structures in the $A_{65}B_{35}$ glass, and thus to its better glass forming ability and resistance against crystallization. Secondly the $A_{80}B_{20}$ data has, for the three slowest-rate cooling curves, a unusual feature that is not present in $c_V(T)$ for the $A_{65}B_{35}$ system in that one sees a small peak in the specific heat that coincides with the maximum of the heating curve, see Fig. 9b. This feature could be a sign of incipient crystallization, e.g. due to the appearance of sub-critically sized nuclei.

Since $D = 2$ simulations require less computational effort that the three dimensional systems, slower cooling and heating rates can be investigated. Figure 10 shows the $D = 2$, $A_{65}B_{35}$ system for scanning rates that vary by four decades and we see that all of them have a well defined glass transition. We note a substantial decrease of the width of the glass transition, in agreement with the data shown in Fig. 9. In fact, in general there is no qualitative difference between this system and the one in $D = 3$ and hence we can conclude that qualitatively the glass transition does not depend on D, if $D \geq 2$.

From Figs. 9 and 10 one recognizes clearly that above T_g the specific heat increases

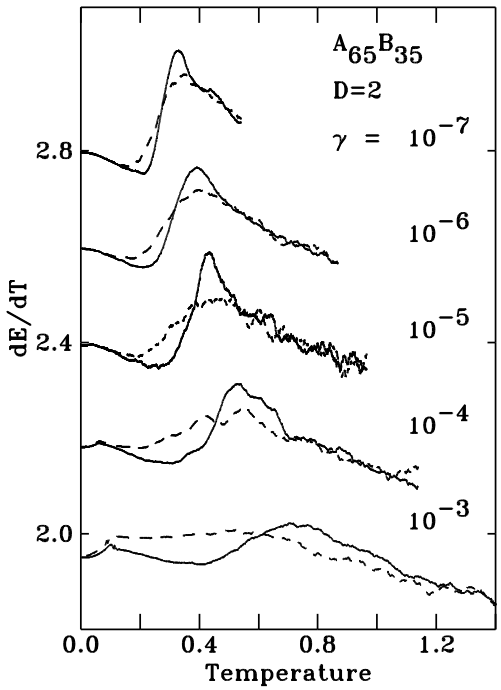

FIG. 10: Constant volume specific heat, per particle, for $A_{65}B_{35}$ in two dimensions upon cooling (dashed lines) followed by heating (solid lines). Curves at rates slower than $\gamma = 10^{-3}$ are shifted up successively by 0.2.

with decreasing temperature, in agreement with previous studies of this Lennard-Jones system [10, 50]. Such a $T-$dependence is not unexpected since the relaxation time shows a significant non-Arrhenius dependence on T [29, 30, 31], i.e. the system can be considered as "fragile" [64], and experimentally it is known that fragile glass-formers usually have a specific heat that increases with decreasing T [65, 66].

Due to this increase of c_V with decreasing T, the excess specific heat $\Delta c_V(T) = c_V^{\rm liquid}(T) - c_V^{\rm glass}(T)$ becomes larger at lower temperatures, in accordance with experimental results [67]. Accordingly the step $\Delta c_V(T_g)$ becomes larger as T_g decreases upon slower cooling. Furthermore we see from Figs. 9 and 10 that the heat flow rises above the specific heat of the supercooled liquid as the glass regains metastable equilibrium when the system is heated to $T > T_g$, an effect that also observed in real experiments and which is due to the kinetics of the glass transition. We compare the $T-$dependence of the specific heat found in the present simulations with experimental results by using normalized scales. Following Tool, we scale the ordinate by converting the specific heat signal into the fictive temperature $T_f(T)$ of the system [49]. For this we have linearly extrapolated the specific heat of the glass

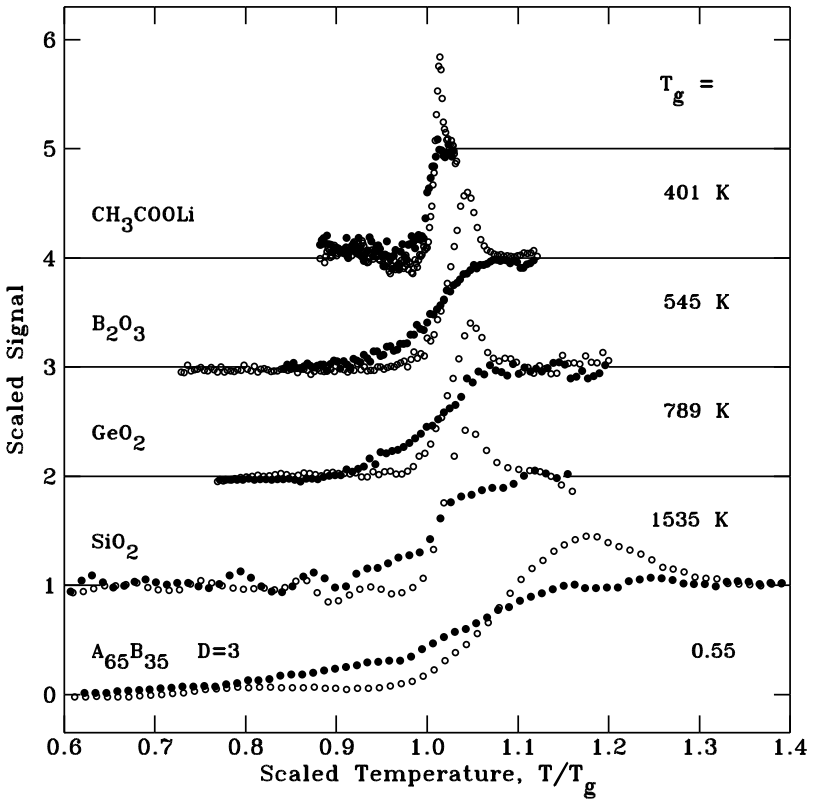

FIG. 11: Comparison of the $D = 3$, $A_{65}B_{35}$, $\gamma = 10^{-6}$ simulation result with the glass transition in experimental systems [51, 68, 69]. For lithium acetate and GeO_2 the data are scaled results from calorimetric experiments, while for B_2O_3 and SiO_2 the curves are based on volume expansion and small angle x-ray scattering data, respectively. Temperature:s are scaled by T_g. Ordinate values are scaled by subtracting the (extrapolated) signal of the glass state and dividing the residual by the (extrapolated) supercooled liquid signal. Curves other than the BMLJ system are shifted up by successive steps of 1.

to the supercooled liquid regime, and the specific heat of the supercooled liquid was extrapolated into to glass regime [50]. One then subtracts the (extrapolated) glass signal from the data as well as from the supercooled liquid curve. Finally one divides the residual curves (cooling and heating) by the residual supercooled liquid curve. The scaled data dT_f/dT is shown as a function of T/T_g in Fig. 11. Here T_g was defined consistently as the value of T_f reached upon cooling to the lowest temperature. Note that by construction the scaled signal goes to zero at low temperatures and to unity at high temperatures. Also included in the graph is the corresponding data from experiments of different glass-formers [51, 68, 69]. The comparison of the data from simulation with the one from experimental shows that

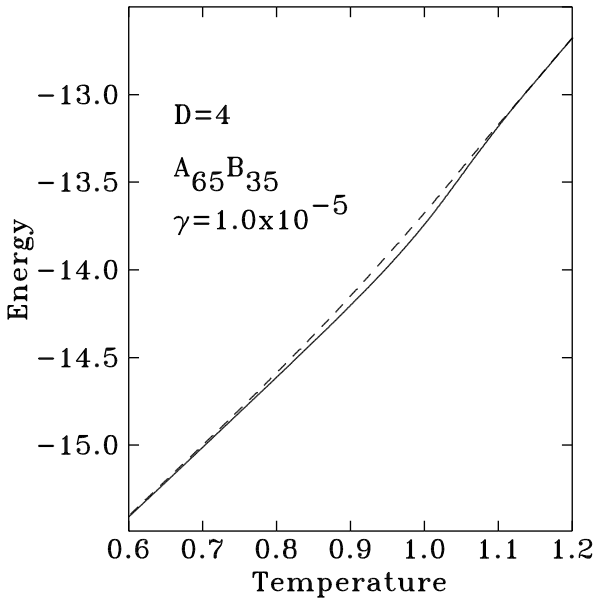

FIG. 12: The total energy per particle for $A_{65}B_{35}$ in four dimensions upon cooling (dashed line) followed by heating (solid line) at rate $\gamma = \mp 1.0 \times 10^{-5}$.

the hysteresis at the glass transition of the BMLJ system reproduces indeed the shape observed in experiments carried out with fragile and strong glass-formers. We also see that the width of the glass transition as observed in the simulation is significantly larger than the one found even in the strongest glass-forming substances, such as SiO_2, and much larger than the fragile glass-former lithium acetate. This difference could have been expected since this width depends not only on the fragility of the glass-former but also on the cooling rate [10], and the temperature scanning rates of the simulations are typically 10^{10} times faster than laboratory rates [1, 7].

In the following we consider the dependence of the hysteresis on temperature scanning rate, composition, and dimensionality of the system in more detail. Figure 12 shows the total energy $E(T)$ upon cooling and heating for the four-dimensional $A_{65}B_{35}$ system. We denote the area of the hysteresis loop between heating and cooling curves as ΔA, and their maximum separation as ΔE. Figure 13 shows these two quantities as a function of temperature scanning rate γ on logarithmic scales. The data points fall, to a good approximation, onto parallel lines, indicating a power-law dependence of ΔA and ΔE on γ. Therefore we fitted the data with the functional form $\Delta A(\gamma) = \Delta A_0(\gamma/10^{-5})^{\alpha}$ and $\Delta E(\gamma) = \Delta E_0(\gamma/10^{-5})^{\epsilon}$, where ΔA_0 and ΔE_0 are the area and the maximum separation

at $\gamma = 10^{-5}$, respectively. The exponents that best fit all data are $\alpha = 0.40 \pm 0.02$ and $\epsilon = 0.17 \pm 0.03$. Table I lists the pre-factors ΔA_0 and ΔE_0. From this table, and from Fig. 13, we can conclude that the hysteresis effect increases with increasing D, in agreement with the result shown in Fig. 8, i.e. that the glass-forming ability of the system increases with its dimensionality.

A similar analysis can also be done for real systems, although of course only for $D = 3$ [68]. It is found that the area and maximum separation of the hysteresis curves also show a power-law dependence on the cooling rate, thus showing that the results from the present simulations are consistent with real experiments. However, these experiments yield exponents of 0.29 for area and 0.15 for the height, i.e. different values from the one found here and hence we can conclude that these exponents are not universal, but material-specific or characteristic of the regime of temperature scanning rate.

Since fragile glass-formers systems have relaxation times $\tau(T)$ that seem to diverge at a finite temperature [64], their effective activation barriers, i.e. the local slope of $\log(\tau)$ vs. $1/T$ is larger than the one for strong glass-formers, if τ has macroscopic values, e.g. 1 second. The temperature range at which the system falls out of equilibrium at the glass-transition is therefore trivially related to the fragility of the system, with fragile (strong) glass-formers showing a transition in a narrow (wide) temperature range. As mentioned above, the present BMLJ system is expected to be a fragile glass-former since its relaxation times show a strongly non-Arrhenius $T-$dependence. Using the power-laws approximations for the scanning rate dependence of the hysteresis loop (Fig. 13), we can obtain a rough estimate for the behavior of the BMLJ systems at laboratory scanning rates ($\gamma = 10^{-15} \approx$ 2K/s, if we identify the A particles as argon atoms). Of course it is highly uncertain whether or not the present BMLJ system avoids crystallization at such slow rates. The width of the glass transition ΔT is proportional to the ratio $\Delta A/\Delta E$ and thus its γ-dependence is given by the exponent $\alpha - \epsilon$. Referring to Fig. 11, one can estimate the width of the hysteresis loop for $A_{65}B_{35}$ at $\gamma = 10^{-6}$ to be $\Delta T = 0.5T_g$. The power-law approximation, with $\alpha - \epsilon \approx 0.23$, predicts then for the laboratory rate a $\Delta T = 0.004T_g$ (or $\Delta T = 0.027T_g$ if using the experimentally derived values $\alpha = 0.29$ and $\epsilon = 0.15$). By comparison, the width of the (fragile) lithium acetate glass curve in Fig. 11 is about 0.04. We conclude that, based on this analysis, the BMLJ system is indeed fragile, in agreement with the data from the $T-$dependence of the relaxation times [29, 30, 31]. Last not least we also can conclude

System	$\Delta E_0 \times 10^3$	$\Delta A_0 \times 10^3$
$A_{65}B_{35}$, $D = 2$	2.1±0.4	8.4±0.7
$A_{65}B_{35}$, $D = 3$	6.6±0.8	31±5
$A_{65}B_{35}$, $D = 4$	16.0±1.5	76±6
$A_{80}B_{20}$, $D = 3$	4.5±0.2	18±2

TABLE I: Values of the pre-factor for the power-law fits $\Delta E = \Delta E_0(\gamma/10^{-5})^{0.17}$ and $\Delta A = \Delta A_0(\gamma/10^{-5})^{0.40}$, representing the height and area of the hysteresis loop in the total energy, respectively.

that the fragility depends on the dimensionality of the system, since the width of the glass transition increases with increasing D (see Fig. 13).

IV. SUMMARY

We have presented the results of molecular dynamics simulations in order to study how the calorimetric glass transition of binary Lennard-Jones systems depends on the cooling rate and the number of dimensions. The BMLJ systems were cooled at a constant rate $-\gamma$, followed by reheating to the ergodic liquid state at rate γ. We find that the composition $A_{80}B_{20}$, a good glass-former in three dimensions, crystallizes in two dimensions if γ is small, whereas the composition $A_{65}B_{35}$ does not crystallize for any dimension at the cooling rates investigated here.

For glasses that have been produced with a given (small) γ we find that the peaks in the radial distribution functions become quickly washed out with increasing dimensionality D, reflecting fewer geometric constraints. In particular the nearest neighbor peak of the radial distribution functions becomes broader, reflecting a wider range of geometric configurations in higher dimensions. This is evidence that the glass-forming ability of the system increases with increasing dimensionality. As D increases, the first peak in the radial distribution function shifts closer to the central atom due to force exerted by the second-nearest neighbors on the nearest neighbors, thus resulting in a stronger $T-$dependence of the pressure. At low temperatures the $T-$dependence of the constant volume specific heat of the glass is very close to the one of a one-component Lennard-Jones crystal, showing that the anharmonic

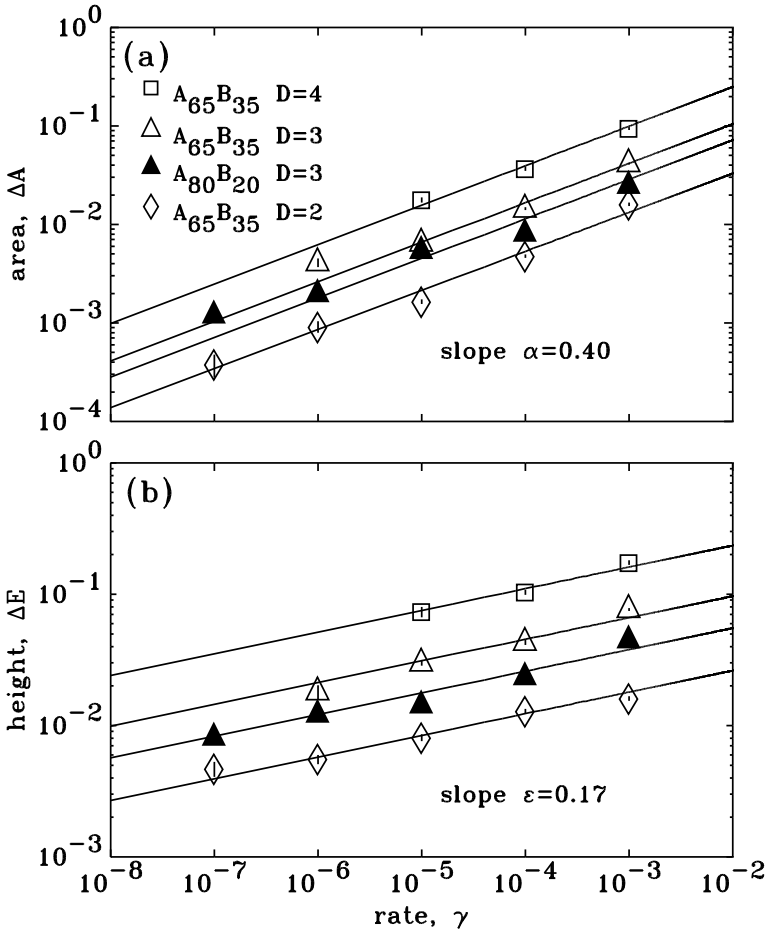

FIG. 13: Area, (a), and height, (b), of the hysteresis loop at the glass transition versus the scanning rate on logarithmic scales for different compositions and number of spatial dimensions. Symbols correspond to the systems presented in the upper left corner of (a). Solid lines are fits to the power laws $\Delta A = \Delta A_0(\gamma/10^{-5})^{\alpha}$ for (a) and $\Delta E = \Delta E_0(\gamma/10^{-5})^{\epsilon}$ for (b).

effects in glasses and crystals are quite similar.

A glass transition was observed in two, three and four dimensions, whereas no glass transition is observed in one dimension. For $D = 1$ the specific heat curve resembles at all temperatures the one of the supercooled liquid for $D \geq 2$, and thus we conclude that the one dimensional system behaves kinetically like a liquid down to $T = 0$.

For the systems that show a glass-transition we find a hysteresis loop (cooling and heating cycle) in the energy per particle as well as in the pressure of the system. At a given cooling rate the area of this loop and the temperature at which it occurs increase with increasing D. Thus this is further evidence that increasing dimensionality raises the glass-forming ability

of the system.

The glass transition becomes sharper with decreasing temperature scanning rate and thus the hysteresis loop shrinks. Power-laws can be used to fit scanning rate dependence of the area and height of these loops. The exponents describing this γ-dependence seem to be independent of composition or dimensionality. A similar analysis of experimental data indicate that these exponents are not universal, but appear to be specific for the system considered.

V. ACKNOWLEDGMENTS

The Natural Sciences and Engineering Research Council of Canada (NSERC) has supported this work through a discovery grant. S.P. and D.St-O. especially thank NSERC for Summer Undergraduate Research Awards. We gratefully acknowledge the Mount Allison Cluster for Advanced Research (TORCH) for allocations of computer resources.

---

[1] H. N. Ritland, J. Amer. Ceram. Soc. **37**, 370 (1954).

[2] C. Y. Yang, D. E. Sayers and M. A. Paesler, Phys. Rev. B **36**, 8122 (1987).

[3] C. T. Limbach and U. Gonser, J. Non-Cryst. Solids **106**, 399 (1988).

[4] L. C. E. Struik, *Physical Aging in Amorphous Polymers and Other Materials* (Elsevier, Amsterdam, 1978);

[5] G. P. Johari, A. Hallbrucker and E. Mayer, J. Phys. Chem. **93**, 2648 (1989).

[6] H. Miyagawa and Y. Hiwatari, Phys. Rev. A **40**, 6007 (1989).

[7] R. Brüning and K. Samwer, Phys. Rev. B, **46**, 11318 (1992).

[8] I. M. Hodge, J. Non-Cryst. Solids **169**, 211 (1994).

[9] C. Levelut, N. Gaimes, F. Terki, G. Cohen-Solal, J. Pelous J., and R. Vacher, Phys. Rev. B **51**, 8606 (1995).

[10] K. Vollmayr, W. Kob, and K. Binder, J. Chem. Phys. **105**, 4714 (1996).

[11] C. S. Liu, Z. G. Zhu, J. C. Xia, and D. Y. Sun, J. Phys.: Condens. Matter **13**, 1873 (2001).

[12] J. Buchholz, W. Paul, F. Varnik, and K. Binder, J. Chem. Phys. **117**, 7364 (2002).

[13] B. M. Lee, H. K. Baik, B. S. Seong, S. Munetoh, and T. Motooka, Comp. Mat. Sci. **37**, 203 (2006).

[14] S. Le Roux and P. Jund, J. Phys.: Condens. Matter **19**, 196102 (2007).

[15] S. Streit-Nierobisch, C. Gutt, M. Paulus, and M. Tolan, Phys. Rev. B **77**, 041410 (2008

[16] J. Zarzycki (Ed.) *Materials Science and Technology, Vol. 9*, (VCH Publ., Weinheim, 1991).

[17] W. Götze and L. Sjögren, *Rep. Prog. Phys.* **55**, 241 (1992).

[18] M. D. Ediger, C. A. Angell, and S. R. Nagel, J. Phys. Chem. **100**, 13200 (1996).

[19] P. G. Debenedetti, *Metastable Liquids* (Princeton University Press, Princeton, 1997).

[20] W. Götze, *J. Phys.: Condens. Matter* **10**, A1 (1999).

[21] L. F. Cugliandolo, p. 367 in *Lecture Notes for "Slow relaxations and nonequilibrium dynamics in condensed matter", Les Houches July, 1-25, 2002; Les Houches Session LXXVII* Eds. J.-L. Barrat, M. Feigelman, J. Kurchan, and J. Dalibard (Springer, Berlin, 2003).

[22] S.P. Das, Rev. Mod. Phys. **76**, 785 (2004).

[23] K. Binder and W. Kob *Glassy Materials and Disordered Solids: An Introduction to Their Statistical Mechanics* (World Scientific, Singapore, 2005).

[24] A. H. Marcus, J. Schofield, and S. A. Rice, Phys. Rev. E **60**, 5725 (1999).

[25] H. König, R. Hund, K. Zahn, and G. Maret, Europ. Phys. J. E **18**, 287 (2005).

[26] F. Thalmann, J. Chem. Phys. **116**, 3378 (2002).

[27] G. Parisi and F. Zamponi, J. Stat. Mech. Theor. Exp. P03017 (2006).

[28] M. Tarzia, J. Stat. Mech. Theor. Exp. P01010 (2007).

[29] W. Kob and H. C. Andersen, Phys. Rev. Lett. **73**, 1376 (1994).

[30] W. Kob and H. C. Andersen, Phys. Rev. E **51**, 4626 (1995).

[31] W. Kob and H. C. Andersen, Phys. Rev. E **52**, 4134 (1995).

[32] M. Nauroth and W. Kob, Phys. Rev. E **55**, 657 (1997).

[33] T. Gleim, W. Kob, and K. Binder, Phys. Rev. Lett. **81**, 4404 (1998).

[34] F. Sciortino, W. Kob, and P. Tartaglia, Phys. Rev. Lett. **83**, 3214 (1999).

[35] L. Berthier, Phys. Rev. E **69**, 020201 (2004).

[36] R. K. Murarka and B. Bagchi, Phys. Rev. E **67**, 41501 (2004).

[37] E. Flenner and G. Szamel, Phys. Rev. E **72**, 031508 (2005).

[38] L. Berthier and R. L. Jack, Phys. Rev. E **76**, 041509 (2007).

[39] S. Ranganathan, J. Phys.: Condens. Matter **6**, 1299 (1994).

[40] M. M. Hurley and P. Harrowell, Phys. Rev. E **52**, 1694 (1995).

[41] D. N. Perera and P. Harrowell, Phys. Rev. E **59**, 5721 (1999).

[42] B. Doliwa and A. Heuer, Phys. Rev. E **61**, 6898 (2000).

[43] B. Doliwa and A. Heuer, J. Phys.: Condens. Matter **15**, S859 (2003).

[44] L. Santen and W. Krauth, Nature **405**, 550 (2000).

[45] M. Bayer, J. M. Brader, F. Ebert, M. Fuchs, E. Lange , G. Maret G, R. Schilling, M. Sperl, and J. P. Wittmer, Phys. Rev. E **76**, 011508 (2007).

[46] D. Frenkel and B. Smit, *Understanding Molecular Simulation: ¿From Algorithms to Applications* (Academic Press, San Diego, 1996).

[47] F. Pfender and G. M. Ziegler, Notes of the AMS **51**, 873 (2004).

[48] P. Ballone and B. Montanari, Phys. Rev. E **76**, 011508 (2002).

[49] A. Q. Tool, J. Am. Ceram. Soc. **29** 240 (1946).

[50] F. Sciortino, W. Kob, and P. Tartaglia, J. Phys.: Condens. Matter **12**, 6525 (2000).

[51] R. Brüning and M. Sutton, J. Non-Cryst. Solids **205-207**, 480 (1996).

[52] W. Kob and R. Schilling, J. Phys. A **23**, 4673 (1990).

[53] J.-P. Hansen and I. R. McDonald, *Theory of Simple Liquids* (Academic, London, 2006).

[54] K. Vollmayr, W. Kob and K. Binder, Europhys. Lett. **32**, 715 (1995).

[55] K. Vollmayr, W. Kob and K. Binder, Phys. Rev. B **54**, 15808 (1996).

[56] T. F. Middleton, J. Hernandez-Rojas, P. N. Mortenson, and D. J. Wales, Phys. Rev. B **64**, 184201 (2001).

[57] J. R. Fernandez and P. Harrowell Phys. Rev. E **67**, 011403 (2003).

[58] N. W. Ashcroft and N. Mermin, *Solid Stats Physics* (Holt-Saunders, Tokyo, 1976).

[59] S. H. Aly, Egypt. J. Sol. **23**, 217 (2000).

[60] K. Westera and E. R. Cowley, Phys. Rev. B, **11**, 4008 (1975).

[61] E. R. Cowley, Phys. Rev. B **28**, 3160 (1983).

[62] R. Brüning, E. Irving, and G. LeBlanc, J. Appl. Phys. **89**, 3215 (2001).

[63] R. Brüning and M. Sutton, Phys. Rev. B, **49**, 3124 (1994).

[64] R. Böhmer and C. A. Angell, p. 11 in *Disorder Effects on Relaxation Processes* Eds. R. Richert and A. Blumen (Springer, Berlin, 1994)

[65] C. Alba, L. E. Busse, D. J. List, and C. A. Angell, J. Chem. Phys. **92**, 617 (1990)

[66] C. A. Angell, P. H. Poole, and J. Shao, Nuovo Cimento D **16**, 993 (1994).

[67] C. A. Angell, Pure Appl. Chem. **63**, 1387 (1991).

[68] R. Brüning, J. Non-Crystal. Solids **330**, 13 (2003).

[69] R. Brüning, C. Levelut, A. Faivre, R. Le Parc, F. Bley, and J. Hazemann, Europhys. Lett. **70**, 211 (2005).